Title: Cypate and cypate-glucosamine as near infrared (NIR) fluorescent probes for *in vivo* tumor imaging

Authors: Mona Doshi, Daniel A Nierenberg, Orielyz Flores-Fernandez, Pragney Deme, Edilu Becerra, Annette R Khaled, Sampath Parthasarathy

Affiliation: Burnett School of Biomedical Sciences, College of Medicine, University of Central Florida. 6900 Lake Nona Blvd. Orlando, FL 32827.

Running title: Cypate-glucosamine for *in vivo* imaging

Name and complete address of corresponding author

Sampath Parthasarathy, Ph.D., MBA.

Burnett School of Biomedical Sciences, College of Medicine,

University of Central Florida.

6900 Lake Nona Blvd. Orlando, FL 32827.

Tel: (407) 266-7121;

Fax: (407) 266-7002

Email: spartha@ucf.edu

Number of text pages: 37

Number of tables: 0

Number of schemes: 1

Number of figures: 7

Number of references: 60

Number of words in abstract: 248

Number of words in introduction: 749

Number of words in discussion: 1483

Abbreviations:

Chemical exchange saturation transfer - CEST

Computerized tomography - CT

Cypate-1-glucosamine - cy-1-glu

Cypate-2-glucosamine - cy-2-glu

Dichloromethane - DCM

Diisopropylethylamine - DIEA

Dimethylformamide - DMF

Dimethylsulphoxide - DMSO

2[F-18] Fluoro-2-Deoxy-D-Glucose - FDG

Fourier-transform Infrared Spectroscopy - FTIR

1-Hydroxybenzotriazole hydrate - HOBt

Liquid chromatography and mass spectrometry - LC-MS

Magnetic resonance imaging - MRI

N,N,N′,N′-Tetramethyl-O-(1H-benzotriazol-1-yl)uronium hexafluorophosphate - HBTU

2-(N-(7-Nitrobenz-2-oxa-1,3-diazol-4-yl)Amino)-2-Deoxyglucose - NBDG

Near infrared - NIR

Nuclear Magnetic Resonance - NMR

Palmitic acid - PA

Positron emission tomography - PET

Saturated cypate - sat-cy

Abstract:

Near infrared (NIR) imaging is a promising technique for use as a non-invasive and sensitive diagnostic tool. While the NIR fluorescently labeled glucose analog glucosamine (cypate-glucosamine) has applications in pre-clinical imaging, the transport pathways and fate of this probe in tissues remain unaddressed. Here, we have synthesized and characterized cypate and cypate-glucosamine conjugate (cy-2-glu), and investigated the probable transport pathways of these probes *in vitro* and *in vivo*. We compared uptake of the probes in the presence and absence of excess D-glucose, 'saturated cypate' and palmitic acid in two normal - cancer cell line pairs: lung cancer (A549) - normal (MRC9), and prostate cancer (DU145) - normal (BPH). Breast cancer (MDA-MB-231) and liver cancer (HepG2) cell lines were also examined. Results support utilization of the glucose transport pathway by cy-2-glu and fatty acid transport pathway by cypate. Mass spectrometry data on the *in vitro* extracts revealed deamidation of cy-2-glu in prostate and liver cells, suggesting release of glucosamine. *In vivo* biodistribution studies in mice engrafted with breast tumors showed a distinct accumulation of cy-2-glu in liver and tumors, and to a lesser extent in kidneys and spleen. A negligible accumulation of cypate alone in tumors was observed. Analysis of urine extracts revealed renal excretion of the cy-2-glu probe in the form of free cypate, indicating deamidation of cy-2-glu in tissues. Thus, investigation of the metabolic pathways used by NIR probes such as cy-2-glu, advanced their use in the detection and monitoring of tumor progression in preclinical animal studies.

Introduction:

Optical methods using near-infrared (NIR) probes, in the spectral range of 700 nm-2500 nm, are of interest due to features like flexibility of use, cost-effectiveness and minimal toxicity. A promising NIR probe application is pre-clinical *in vivo* tumor imaging due to, 1) low auto-fluorescence from biomolecules (ensuring minimum background light), 2) low tissue absorbance (delivering high penetration of the light), 3) low light scattering (leading to high signal to noise ratio), and 4) non-radiation applications (limiting deleterious effects from radiation-based therapies). Non-invasive tumor detection by NIR probes has proven highly sensitive within various animal studies (Haque et al. 2017; Hilderbrand and Weissleder 2010; Luo et al. 2011). Targeted and activated imaging of cancers was reported using NIR dyes (Owens et al. 2016; Hilderbrand and Weissleder 2010; Escobedo et al. 2010). Conventional NIR imaging molecules include cyanine (Kim et al. 2005; Peng et al. 2005), phthalocyanine, porphyrine (Srinivasan et al. 2003; Tanaka, Shin, and Osuka 2008; Xie et al. 2009), squaraine (Nakazumi et al. 2005; Umezawa, Citterio, and Suzuki 2008; Volkova et al. 2007), and BODIPY (boron-dipyrromethene) (Donuru et al. 2010; Umezawa et al. 2009; Umezawa et al. 2008). Of these, the cyanine dye, cypate has excellent optimal properties with a high extinction coefficient (224,000 $(mol/L)^{-1}cm^{-1}$) and two carboxylic groups suitable for conjugation with amine or hydroxyl groups.

Due to cypate's low tissue absorbance, and thus minimal background it is well suited for *in vivo* imaging. This was first shown in studies conducted by Achilefu et al. (Achilefu et al. 2005; Achilefu et al. 2000) in which peptide-conjugated cypate probes that targeted integrins, molecules involved in tumor-induced angiogenesis and metastasis, were tested for NIR imaging of A549 cells in nude mice. Subsequent studies have used glucosamine-conjugated cypate moieties for cancer-related imaging. Ye et al. evaluated combinations of cypate-conjugated glucosamine moieties and observed their biodistribution in pancreatic cancer-bearing mice (Ye et al. 2005) and determined that the number of glucosamine moieties conjugated to cypate could influence cypate uptake in tumors in a similar manner. Cheng et al. studied Cy5.5-D-glucosamine (Cy5.5-2DG) and 2-(N-(7-Nitrobenz-2-oxa-1,3-diazol-4-yl)Amino)-2-Deoxyglucose

(NBDG) probes, showing that NBDG, which has a smaller molecular weight compared to the Cy5.5-2DG, was more likely to utilize glucose-based transport in U87MG human glioblastoma cells (Cheng et al. 2006). Jing et al. examined the biodistribution and clear routes of glucosamine-conjugated hydrophilic ICG (Indocyanine green) and glucosamine-conjugated lipophilic cypate probe in breast cancer and glioblastoma-bearing mice to find that ICG-glucosamine probe cleared out faster than cypate-glucosamine probe (Jing et al. 2012). Korotcov et al. studied glucosamine-conjugated cypate biodistribution in prostate cancer-bearing mice, finding that cypate conjugated to two glucosamine moieties demonstrated higher tumor uptake and retention time than cypate conjugated to one glucosamine moiety (Korotcov et al. 2012) .

As indicated by the above studies, cypate and the cypate-conjugated probes have use in cancer imaging. Their optimum use depends on the biophysical properties of the probe (hydrophobicity, lipophilicity, molecular weight, number of targeting molecules etc.). Additionally, knowledge of their transport pathways is equally important to make advancements in optimal probe design. One of the hallmarks of cancer is an altered metabolism leading to increased glucose uptake called the Warburg effect (Liberti and Locasale 2016; Warburg 1925; Hanahan and Weinberg). This phenomenon underlies malignant tissue detection by PET scan using 2[F-18] Fluoro-2-Deoxy-D-Glucose (FDG) (Hoh et al. 1993; Som et al. 1980; Lapela et al. 1995; Phelps 2000; Flamen et al. 2000). CEST MRI (chemical exchange saturation transfer) also employs D-glucose, FDG, 2-deoxy-D-glucose, 3-O-methyl-D-glucose, glucosamine and N-acetyl glucosamine molecules (Chan et al. 2011; Rivlin and Navon 2018; Vinogradov, Sherry, and Lenkinski 2013; Walker-Samuel et al. 2013; Wu et al. 2016; Zhang, Trokowski, and Sherry 2003). Hence use of these methods shows the effectiveness of targeting glucose metabolism for imaging probes, supporting our approach with cypate. However, despite their value in imaging, the glucose- and carboxylate-based transport pathways of such imaging probes has not been investigated. To this end, we examined the biophysical characteristics of cypate and cypate-glucosamine (cy-2-glu) as well as their optical properties. We determined whether glucosamine-conjugated cypate transport into cells is glucose-

dependent or carboxylate-dependent. We also characterized and analyzed the molecular changes in cypate and cy-2-glu in animals to determine the retention time and fate of the probes. Understanding the transport mechanisms of cypate and cy-2-glu in malignant and non-malignant cells adds needed information on how the chemical structure of NIR probes affects their biodistribution. This information will advance the tissue-specific imaging and drug delivery application of NIR probes like cy-2-glu, demonstrating that these conjugates have translational benefits.

Materials and methods:

Materials

1,1,2-trimethyl benz[e]indole, 3-bromopropanoic acid, 1,2-dichlorobenzene, dichloromethane (DCM), acetonitrile, sodium acetate, glutaconaldehyde dianil hydrochloride, diisopropylethylamine (DIEA), acetic anhydride, dimethylformamide (DMF), N,N,N′,N′-Tetramethyl-O-(1H-benzotriazol-1-yl)uronium hexafluorophosphate (HBTU), 1-Hydroxybenzotriazole hydrate (HOBt), glucosamine hydrochloride, dimethylsulphoxide (DMSO), acetone, Pd/C (10% Pd) and LC-MS solvents were purchased from Sigma Aldrich (St. Louis, MO, USA). Hydrochloric acid was purchased from Fisher (Pittsburgh, PA, USA). Diethyl ether was purchased from VWR (Radnor, PA, USA). Ethanol was purchased from Pharmaco-Aaper (Brookfield, CT, USA).

Methods

1. Synthesis of cypate, cy-2-glu and saturated cypate (sat-cy)

1.1 Synthesis of 1,1,2-trimethyl benz[e]indole-3-propanoic acid:

1,1,2-trimethyl benz[e]indole-3-propanoic acid was synthesized as previously described (Ye et al. 2005) Briefly, 4 g of 1,1,2-trimethyl benz[e]indole (19.11 mmoles) were dissolved in 20 mL of 1,2-dichlorobenzene in a conical flask to obtain a dark yellow solution. 4 g of 3-bromopropanoic acid (26.15 mmoles) were added to the above solution. This solution was heated to 110°C with continuous stirring for

18 hrs before cooling to room temperature upon which the solution turned dark grey-green. This solution was vacuum filtered through Whatman™ filter paper. The white colored precipitate was washed with DCM by trituration and transferred to a glass petri dish. This synthesis yielded 5.5 g of product.

1.2. Synthesis of cypate:

Cypate was synthesized as previously described (Ye et al. 2005). Briefly, 4.1 g of 1,1,2-trimethyl benz[e]indole-3-propanoic acid (synthesized as described above) was added to a 50 mL acetonitrile-water (47.5 mL acetonitrile + 2.5 mL DI water) solvent system in a round bottom boiling flask. 1.6 g sodium acetate was added to this solution and refluxed at 170°C. In a conical flask, 1.42 g (4.98 mmoles) of glutaconaldehyde dianil hydrochloride was dissolved in 10 mL DCM. While this solution was kept on ice, 1.3 g (10 mmoles) of DIEA was added to it and continued to be kept on ice. In a separate glass vial, 0.6 g of acetic anhydride was mixed in 2.5 mL of DCM. This solution was then added dropwise to the solution containing glutaconaldehyde dianil hydrochloride and stirred at room temperature at a speed of 100 rpm for 1 hr. After mixing, the resultant mixture was added dropwise to the refluxing solution listed above. The reflux was continued for 16 hrs at 170°C. The dark green precipitate formed was filtered through a glass funnel with Whatman™ filter paper. It was washed with acetonitrile, 5% hydrochloric acid and finally with ether. The product was then transferred into a glass petri dish and air-dried for two days. The clumps were separated with a spatula to obtain a dark green fine cypate powder.

1.3. Synthesis of cy-2-glu

Cypate was conjugated to glucosamine as previously described (Ye et al. 2005). Briefly, 30 mg of cypate (0.048 mmoles) were dissolved in 5 mL DMF in a round bottom flask. 41 mg of HBTU were dissolved in 1 mL of DMF and added to the cypate solution. 14.8 mg of HOBt (0.096 mmoles) were dissolved in 1 mL DMF and added to cypate solution. The final volume of this solution was brought to 10 mL by adding DMF. This solution was then chilled to -5°C. In a glass vial, 48 mg of glucosamine (0.266 mmoles) were dissolved in 2 mL DMSO and 76 µL of DIEA (0.436 mmoles) were added to it. The glucosamine solution

was added to the cold cypate solution in one portion and stirred at room temperature for 2 hrs. The reaction mixture was added to 50 mL of ether in a conical flask under vigorous stirring. Upon product precipitation, excess ether was decanted. To remove DMSO completely from the product, acetone was added to the precipitate and after briefly shaking, the acetone was removed to prevent product dissolution. The product was placed in a glass petri dish and air-dried for one day to yield 23.8 mg of crystalline cy-2-glu.

1.4. Synthesis of non-fluorescent, saturated cypate (sat-cy)

For subsequent cell culture experiments involving the uptake of the NIR fluorescent probe cypate, a non-fluorescent, saturated cypate (sat-cy) was synthesized to act as a competitive inhibitor. To synthesize sat-cy, 1 mg of cypate was dissolved in 2 mL ethanol in a 5 mL round bottom flask and approximately 1 mg of Pd/C (10% Pd) was added. In a glass cylinder, zinc granules were mixed with 50 mL of 6N hydrochloric acid. Once hydrogen gas formed, it was passed through the reaction mixture overnight while stirring at room temperature. The reaction mixture was then filtered and centrifuged to remove Pd/C. Ethanol was evaporated completely to yield sat-cy.

2. Cell culture and experiments

2.1 Cell culture:

A549 (human lung cancer), MRC9 (human lung normal), BPH (human prostate normal), MDA-MB-231 and luciferase-expressing MDA-MB-231-luc2 (human breast cancer), and HepG2 (human liver cancer) cell lines were cultured in DMEM media with 10% FBS in humidified atmosphere of 95% air/5% CO_2 at 37°C. DU145 (human prostate cancer) cells were grown in RPMI media supplemented with 10% FBS in humidified atmosphere of 95% air/5% CO_2 at 37°C. THLE-2 (normal human liver) cells were cultured in Airway Epithelial Cell Basal Medium (ATCC - Manassas, VA) supplemented with a bronchial epithelial cell growth kit (ATCC) and grown under a humidified atmosphere. Cell lines were purchased from ATCC

and frozen after three passages. All cell lines were used from frozen stocks for no more than 9-12 passages.

2.2 *In vitro* cypate and cy-2-glu uptake assays

1×10^6 of each cell type were plated on individual 35 mm glass bottom petri dishes. After 24 hrs, cell lines were incubated for 2 hrs with a 10 µM solution of cypate/cy-2-glu in phenol red free media. Following treatment, cells were either washed 3× with PBS and fixed with 4% paraformaldehyde for imaging or had their intracellular cypate and cy-2-glu contents collected for spectroscopy and/or LC-MS analysis. For intracellular cypate and cy-2-glu collection, treated cells were harvested with 0.25% trypsin, centrifuged and washed with PBS. The pellet was resuspended in 1 mL of methanol/acetonitrile/water solvent system (2:2:1, v/v) and vortexed for 30 sec. Cells were then freeze-fractured by chilling the samples in liquid nitrogen for 1 min, allowing them to return to room temperature and then sonicated them for 10 min. The above procedure was repeated 3× to ensure maximum extraction of the dyes. After this, the samples were placed in -20°C for 1 hr to precipitate the cellular matrix. The samples were centrifuged for 15 min at 13,000 rpm at 4°C. The supernatant was collected and evaporated to dryness under gentle stream of nitrogen gas (N_2). The residues were dissolved in 100 µL of acetonitrile/water (1:1, v/v) to remove any remaining cell debris. Samples were centrifuged at 13,000 rpm for 15 min at 4°C. The supernatant was separated and dried completely under N_2. The dried samples were resuspended in 400 µL of methanol and stored until further analysis.

2.3 Competitive uptake of cypate and cy-2-glu with excess D-glucose, sat-cy and PA.

To assess which transport mechanisms may be involved in the cellular uptake of cypate and cy-2-glu, uptake assays as described above in Methods section 2.2 were carried out in the presence of excess D-glucose, sat-cy or PA. For each experiment, cells were cultured in DMEM alone or supplemented with 5 mM D-glucose, 100 µM sat-cy or 100 µM PA in phenol red-free media for 2 hrs. Following treatment,

cells were fixed for imaging or had their intracellular cypate and cy-2-glu contents collected for analysis via spectroscopy and/or LC-MS.

3. Animal experiments

3.1 *In vivo* D-glucose competition for cy-2-glu uptake.

To access how D-glucose competes against cy-2-glu uptake *in vivo*, tumor were implanted into mice. Briefly, 100 µL of 8×10^5 luciferase-expressing breast cancer cells (MDA-MB-231 Luc2) in Matrigel (Corning) were implanted orthotopically in the mammary fat pad of JAX (Jackson Laboratory) Foxn1nu/Foxn1nu nude 2.5-month-old female mice using a 26.5G BD 1 mL insulin U-100 syringe. As a pilot study, two nude mice with breast tumors of comparable size (~250 mm^3) were selected. In one of the mice, 100 µL of 20 mM D-glucose in PBS was injected intravenously. After 15 min, 10 nmoles of cy-2-glu in 100 µL PBS were administered in both mice through tail vein injection. After 20 min, 15 mg/mL luciferin in PBS (100 µL) was injected in the intraperitoneal cavity. Imaging was performed in a Bruker Xtreme *in vivo* imaging system with Bruker MI SE software. The mice were anesthetized using 2% isoflurane. Animals were then imaged as described below. Since the fluorescence intensity from liver was very high, it was impeding imaging of other organs or tissues. The liver area was covered with a black strip and the exposure time for fluorescence was increased to 2 min to collect maximum signal from rest of the organs. The parameters for bioluminescence and reflectance images remained unchanged. Overlaying of the images was done in the same software.

3.2. Biodistribution of cy-2-glu and cypate in organs:

8×10^5 luciferase-expressing breast cancer cells (MDA-MB-231 Luc2) were implanted orthotopically in the mammary fat pad of JAX (Jackson Laboratory) Foxn1nu/Foxn1nu nude 2.5-month-old female mice. 10 nmoles of cy-2-glu/cypate in 100 µL PBS was injected intravenously in these mice. Experiments were performed at 1 h post-injection and then every 24 hrs for six days. For each time point, three (3) mice

were used with similar-sized tumors (~250 mm^3). 15 min prior to imaging, urine was collected from the mice and kept in the refrigerator for until further analysis. 15 mg/mL luciferin in PBS (100 µL) was injected in the intraperitoneal cavity 10 min prior to *in vivo* imaging. Mice were anesthetized with 2% isoflurane and imaged as described below. A black strip was used again to block the liver as described above.

After *in vivo* imaging, mice were sacrificed by cervical dislocation and organs were isolated and imaged. Following *ex vivo* imaging, cy-2-glu and cypate were extracted from the organs and urine by cutting the organs into small pieces in glass petri dishes with small scissors and transferring them into homogenizing tubes. 1 mL DI water was added to the tubes and samples were homogenized for 5 min. Following this, 3 mL of methanol were added to each tube and samples were homogenized again for 5 min. These solutions were centrifuged for 10 min at 3000 rpm. The supernatants were collected and stored at 4°C overnight to allow precipitate formation. The solutions were centrifuged and the supernatant were collected and dried with N_2 gas. 400 µL of methanol were added to dried samples and centrifuged again. These collected supernatants contained only cy-2-glu or cypate. For urine extraction, 500 µL of urine were collected in a glass tube. 1 mL DI water and 2 mL methanol were then added to this. After precipitate formation, the samples were centrifuged and the supernatants were collected. The supernatants were dried with N_2 gas and 400 µL of methanol were added. Solution spectroscopy and mass spectrometry were performed on the organ and urine extraction samples. All animal work was conducted under the approval of the Institutional Animal Care and Use Committee (IACUC) of the University of Central Florida.

4. Chemical Characterization

4.1 Spectroscopy:

Absorption was analyzed via Ultraviolet–visible (UV-vis) spectroscopy performed in methanol in a 1 cm path length sub-micro quartz cuvette from Spectrecology (Wesley Chapel, FL, USA) with a 6850 Jenway spectrophotometer using Prism software. The fluorescence spectroscopy was performed in methanol in a

1 cm path length sub-micro quartz cuvette with PTI QM-400 fluorimeter (Horiba, Canada) using FelixGX 4.3.6904 software. The detectors used to collect the fluorescence from the samples were 1) multimode photomultiplier tube (PMT) detector for UV-visible range (135-700 nm) and 2) TE cooled InGaAs detector for the NIR range (700-1700 nm). The acquisition time was 0.5 sec at 1 nm interval. Fourier-Transform Infrared Spectroscopy (FTIR) was used to analyze the spectra of the cypate and cy-2-glu samples and was recorded with a Perkin Elmer Spectrum 100.

4.2 Liquid chromatography and mass spectrometry (LC-MS)

An Agilent 1200 series high performance liquid chromatography (HPLC) system consisting of a G1379B degasser, a G1311A quaternary pump, an HTC PAL autosampler and a G1316A column compartment coupled to a 6520 quadrupole time of flight (QTOF) mass spectrometer (Agilent Technologies, CA, USA) was used to characterize and analyze the samples. Compounds were separated on Zorbax Eclipse Plus C18 (150 mm L× 4.6 mm ID, 5 µm PS) column using a binary mobile phase gradient program to elute the components pump- A: acetonitrile and pump-B: water, both containing 0.1% HCOOH. The gradient program was as follows: 90% B: 0–5 min; 10% B: 5–12 min; 10% B, 12–18 min; 90% B: 18-18.1; 10% B: 18.1–23 min. At the end of each run, the column was washed for 3 min with a solvent composition consisting, 50% isopropyl alcohol, 30% methanol, 20% water and 0.1% HCOOH (v/v). The column was operated at 40°C with a constant mobile phase flow rate of 750 µL/min.

The mass spectrometer was operated in electrospray ionization (ESI) positive (+) mode over a mass range of 50-1700 m/z. The mass spectrometer was tuned and calibrated at 4 GHz high resolution mode at low mass 50-1700 m/z range with a manufacturer calibration solution (Agilent, # G1969-85000, CA, USA). The reference mass solution was continuously infused through the second nebulizer to ensure better mass accuracy throughout the analysis. ESI source parameters were optimized and operated under the following conditions: Capillary voltage: 3.5 kV; nitrogen was used as a drying and nebulizer gas and the values were set at 13 L/min and 55 psi, respectively; the source temperature was set at 320°C, Fragmentor

and skimmer voltages were set at 100 V and 65 V, respectively. The MS data were collected and processed using MassHunter qualitative analysis software version B.07.00.

5. Imaging

5.1 Confocal microscopy

Confocal microscopy was performed on *in vitro* cell culture experiments which are described above. A Zeiss AXIO Observer.Z1 microscope with a Zeiss LSM 710 laser system was used for imaging. The images were acquired with Zeiss ZEN 2010.B SP1 software. The objective lenses used were Plan-Apochromat 20X/0.8 M27 and Plan-Apochromat 63X/1.40 oil DIC M27. For Z-stack image acquisition of A549 cells, 15 confocal slices at 0.64 µm intervals were acquired. Cypate and cy-2-glu were excited with 647 nm, while sat-cy and PA were excited with 488 nm wavelength.

5.2 *In vivo* and *ex vivo* imaging of whole animals and individual organs

In vivo imaging on mice was performed using a Bruker Xtreme *in vivo* imaging system with Bruker MI SE software. Images were collected in three channels: 1) Fluorescence channel – The excitation wavelength used was 760 nm and the emission was collected with 830 nm long pass (LP) filter with exposure time 2 min. 2) Bioluminescence channel – The bioluminescence from luciferin in the tumor was collected with 2 min exposure time. 3) Reflectance channel – The grey reflectance image was collected with 5 sec exposure time. Since the fluorescence intensity from liver was very high, it was impeding imaging of other organs or tissues. The liver area was covered with a black strip and the exposure time for fluorescence was increased to 2 min to collect maximum signal from rest of the organs. The parameters for bioluminescence and reflectance images remained unchanged. Overlaying of the images was done in the same software. These three images were overlaid and analyzed for co-localization of cy-2-glu/cypate in the tumors or tissues.

After *in vivo* imaging, mice were sacrificed by cervical dislocation and organs were isolated and imaged. Organ images were collected in two channels: 1) fluorescence channel - Excitation wavelength used was 760 nm and the emission was collected with 830 nm LP filter using exposure time 2 min. 2) The grey reflectance image was collected with 5 sec exposure time.

6. Statistical analysis

In vitro experiments were run in triplicate with a minimum of three repeats. *In vivo* experiments consisted of n=3 animals per experimental group. Statistical analyses were performed using unpaired Student's *t*-test in GraphPad (GraphPad Software Inc.). Statistical significance considered when $p < 0.05$.

Results:

Synthesis and characterization of cypate and cy-2-glu

The NIR dye cypate and the cypate-glucosamine conjugates were synthesized and recovered as pure products by modifying the procedure reported by Ye et al. (Ye et al. 2005) as described in the Methods section. Cypate-glucosamine contained either one carboxylic acid conjugated to one glucosamine (cy-1-glu), or two carboxylic acids each conjugated to one glucosamine moiety (cy-2-glu) (Scheme 1). The molar ratios for synthesis of cy-1-glu yielded a mixture of cy-1-glu, cy-2-glu and unreacted cypate (Supplementary Fig. 1a), whereas, the molar ratios for synthesis of cy-2-glu resulted in only one product, cy-2-glu (Supplementary Fig. 1b). For this reason, cy-2-glu was used for subsequent studies. We evaluated the optical properties of cypate and cy-2-glu by absorption and fluorescence spectroscopy (Supplementary Fig. 2a,b). Cypate and cy-2-glu absorbance spectra have λ_{max} at 784 nm and a shoulder at 722 nm (Supplementary Fig. 2a). The fluorescence profile of cypate and cy-2-glu starts at 800 nm and tails off at 1000 nm, with two emission maxima, at 831 nm and at 935 nm, depicting a wide NIR spectral window for imaging and diagnostic purposes (Supplementary Fig. 2b). The normalized absorption and fluorescence spectra revealed that conjugation of glucosamine to cypate had no adverse effect on the spectral properties of cypate. Neither the spectral profile nor the maxima of absorbance and fluorescence changed due to the conjugation of glucosamine to cypate, although a slight quenching in cypate was noted (data not shown). We checked the formation of an amide bond between the carboxylic group of cypate and the amine group of glucosamine by recording the FTIR spectrum of cy-2-glu and comparing it with the FTIR spectrum of cypate. A medium band for secondary N-H stretch at 3282 cm^{-1} showed the presence of secondary amide between the carboxylic group of cypate and the amine group of glucosamine (Supplementary Fig. 2c). This band can be seen only in the spectrum of cy-2-glu and is absent in cypate. The expanded spectrum in the region from 2000 cm^{-1} to 700 cm^{-1} revealed C=O stretches and amide bends (Supplementary Fig. 2d). The appearance of C=O amide stretch at 1651 cm^{-1} in cy-2-glu along with the absence of C=O carboxylic acid stretch, which is seen in cypate spectrum at 1718 cm^{-1}, confirmed

amide bond formation between cypate and glucosamine. The appearance of N-H bend I (1618 cm^{-1}) and II (1538 cm^{-1}) in cy-2-glu supported this conclusion. We also performed proton and carbon NMR for structure determination (Supplementary Fig. 3a,b). Once cypate and cy-2-glu probes were synthesized, purified and characterized, we next evaluated the transport pathway of these probes and assessed their biodistribution and elimination *in vivo*.

Competitive inhibition of uptake of cy-2-glu in cancer cell lines, indicates glucose transport pathway involvement

As both glucose and glucosamine are taken up in the cells using glucose transport proteins (Calvo et al. 2010), we determined whether the presence of excess of D-glucose would competitively inhibit the uptake of cy-2-glu. This competitive uptake inhibition was observed in A549, HepG2, DU145 and MDA-MB-231 cell lines (Fig. 1). The fluorescence intensities obtained from the confocal images were used as a direct measurement for *in vitro* cellular uptake of cy-2-glu. Decreases in fluorescence intensities for cy-2-glu in the presence of excess (5mM supplemented) D-glucose as compared to absence of D-glucose (no D-glucose supplementation) (Fig. 1a) serves as evidence of competitive inhibition. Cypate alone was not inhibited in the presence of excess D-glucose (Fig. 1b). Z-stack analysis of A549 cells further showed that the probes did not adhere to the plasma membrane but rather were distributed throughout the interior of cells (Supplementary Fig. 4).

Solution spectroscopy of cellular extracts determined the quantitative uptake of cypate and cy-2-glu. The absorption values at 784 nm and the emission intensities at 831 nm for cy-2-glu (Fig. 1c,d) and cypate (Fig. 1e,f), in presence and absence of excess D-glucose are plotted in bar graphs. As with the confocal images (Fig. 1a,b), the spectroscopy data showed a decrease in absorbance and fluorescence of cy-2-glu in cancer cell lines when excess D-glucose was present in the media. Data from cypate in the presence of excess D-glucose showed negligible change in absorbance and fluorescence. These results suggest that

cy-2-glu uses a transport mechanism involving glucose, while cypate uses a non-glucose-utilizing pathway for transport.

The fluorescence intensities of cy-2-glu and cypate in the non-transformed cell lines, MRC9 and BPH, showed no visible change in the microscopy data, in presence or absence of excess D-glucose. However, the fluorescence spectroscopy data for BPH did reveal a decrease in uptake of cypate in presence of excess D-glucose (Fig. 1e) suggesting that these immortalized cells could be more metabolically active. This is likely the result of higher anaerobic metabolic activity in cancerous tissue in response to the demands of growth under low oxygen conditions (Liberti and Locasale 2016; Warburg 1925; Hanahan and Weinberg ; Warburg 1956). Though cypate lacks sugar moieties, we did observe cypate uptake by cancer cells. One explanation for this could be interactions with cypate carboxylates on the cell surface of cancer cells. The reduced negative charge on the surface of cancer cells as compared to normal or non-transformed cells could lessen the repulsion for carboxylate groups, leading to a higher uptake of cypate. Note however that these findings may just be relevant for cells grown under *in vitro* culture conditions.

We compared the quantitative data of all the cancer and non-transformed cell extracts (Supplementary Fig. 5). The absorbance spectra for cypate and cy-2-glu extracted from these cell lines are shown in Supplementary Fig. 5a,b. with the absorbance and fluorescence maxima of the spectra plotted as a bar graph (Supplementary Fig. 5c,d). These data confirmed the increased uptake of cypate and cy-2-glu in cancer cells in comparison to non-transformed cells.

Competitive uptake inhibition of cypate, indicates involvement of fatty acid transport pathway

To determine whether cypate uses carboxylate transporters for transport and uptake, we performed a competitive uptake inhibition experiment using 1) a fatty acid (palmitic acid, PA), and 2) a non-NIR fluorescent analog of cypate (saturated cypate(sat-cy)).

1) Inhibition with fatty acid, PA: If the carboxylic acid groups on cypate were used for transport purposes, the presence of excess of fatty acid (100 μM), which uses carboxylates for fatty acid transport, would

competitively inhibit the uptake of cypate. To test this, we incubated A549 cells with cypate in the presence of 100 μM PA. Confocal fluorescence images showed reduced fluorescence intensity when PA was present in the media (Fig. 2b). Conversely, when the carboxylic acid groups of cypate were modified (amide bond in cy-2-glu), presence of PA did not result in competitive inhibition of cypate uptake (Fig 2a), indicating that carboxylic acid groups are integral to cypate for transport and cellular uptake.

2) Inhibition with sat-cy as a non-NIR fluorescent analog of cypate:

To further validate that cypate is taken up via fatty acid transporters, we used sat-cy as a non-NIR fluorescent analog of the NIR fluorescent cypate (Fig 3), exploiting the optical properties of cypate. Cypate owes its NIR optical properties to the π-conjugated system present within the molecule. Hence, we disrupted the π-conjugation by reducing the double bonds in the glutaconaldehyde dianil moiety, which acts as the bridge between the two indole molecules. Hydrogenation of two double bonds, added four hydrogen atoms to the molecule, breaking the π-conjugation system, and blue shifting the spectra of cypate. We called this new molecule saturated cypate (sat-cy). The synthesis of sat-cy is depicted in Fig. 3a. The addition of four hydrogen atoms to the cypate molecule was confirmed by mass spectrometry (Fig. 3b,c). The molecular ion, at 625 *m/z* for cypate (Fig. 3b) shifted to a molecular ion at 629 *m/z* for sat-cy (Fig. 3c). Thus, sat-cy has no absorbance or emission in the NIR region (700 - 1000 nm) (Fig. 3d,e). Incubation of A549 cells with excess sat-cy resulted in competitive inhibition of cypate uptake similar to addition of excess PA [Fig. 2a,b (cy-2-glu + sat-cy and cypate + sat-cy)] confirming the use of carboxylic acid groups by cypate for transport and cellular uptake.

Absorbance values and fluorescence intensities obtained via UV-vis and fluorescence spectroscopy of cy-2-glu (Fig. 2c,d) and cypate (Fig. 2e,f) from A549 cell extracts correlated with the data collected from confocal microscopy analysis.

Deamidation of cy-2-glu in prostate and liver cell lines

After determining that cy-2-glu and cypate molecules use different pathways for transport, we next asked if the cypate probes underwent any molecular change once inside of cells. We characterized extracts from cells treated with cypate probes by mass spectrometry and observed that the mass spectra of extracts from DU145 and BPH incubated with cy-2-glu, showed the presence of cypate (625 *m/z*) along with cy-2-glu (947 *m/z*), suggesting hydrolysis of cy-2-glu in these cells (Fig. 4a). Conversely, extracts from these cell lines incubated with cypate only showed the presence of the ion at 625 *m/z* that is related to cypate, suggesting that no molecular changes in cypate occurred (Fig. 4b).

In another experiment, instead of analyzing the cell extracts, we analyzed the metabolites released into cell culture media. For this, we incubated the liver cell line, THLE-2, with cy-2-glu for 2 hrs, before addition of fresh media. The cells were incubated for another 24 hrs. Metabolites released into the culture media were then analyzed via LC-MS. We observed the peak for cypate, indicating release of the dye from cells after cy-2-glu was converted into cypate by hydrolysis (Fig. 4d). We also performed this experiment with the MDA-MB-231 breast cancer cell line (data not shown), but no deamidation was observed. The results show that cy-2-glu is hydrolyzed in the liver but not in the tumors, which has implications for the *in vivo* use of this probe.

In vivo **monitoring of cy-2-glu**

We investigated the accumulation and retention of cypate and cy-2-glu in nude mice orthotopically implanted with MDA-MB-231-luc2 breast cancer cells. Upon detection of tumors, mice were intravenously injected with 10 nmol of cy-2-glu or cypate, and the fluorescence intensity of the probes was monitored *in vivo* for six days. Mice with cy-2-glu were evaluated 1 hr post injection, then every 24 hrs for six days (Fig. 5a). Since the accumulation of cypate alone in the tumor was negligible, we monitored these mice only after 24 hrs post-injection (Fig. 5b). Not unexpectedly, the accumulation of probes in the liver produced a high degree of fluorescence that impeded imaging the fluorescent signal from tumors and other organs (data not shown). To remedy this, the liver area was covered with a black

strip to image the rest of the animal. Overlaying tumor bioluminescence (red) with cy-2-glu/cypate fluorescence (green) resulted in a yellow image (i.e. co-localization) that visualized the accumulation of both signals and indicated the presence of cy-2-glu within tumors. Maximum fluorescence intensity of cy-2-glu in tumors was seen at 24 hrs post-injection, which reduced gradually and almost vanished from the tumor by the sixth day (Fig. 5a). A trace amount of fluorescent signal was still detectable from the liver after day six. The *in vivo* accumulation of cy-2-glu but not cypate within the tumor contrasted with the *in vitro* observation where cypate was equally taken up by the cancer cells. This discrepancy may be due to variances in tissue culture conditions compared to the tumor microenvironment (e.g., nutrient availability).

Ex vivo imaging and extraction of probes for evaluation of biodistribution of cy-2-glu and cypate in various organs

To evaluate the biodistribution of cy-2-glu and cypate in the organs, we performed *ex vivo* imaging of tumors and organs. A subset of mice were euthanized at each time point and had their organs harvested and imaged (Fig. 5c,d). The fluorescence intensities are shown in a gradient manner; red represents the highest intensity, while blue represents the lowest intensity. The liver had the highest accumulation of cy-2-glu and cypate at all time points. Over the six days observed, the fluorescence intensity from cy-2-glu gradually decreased in all the organs (Fig 5c) and almost vanished except within the liver which retained trace fluorescence. The absorbance data of the reconstituted solutions of organ extracts are shown in Fig. 5e and directly correlated with *in vivo* and *ex vivo* image analysis. The concentrations of cy-2-glu in the organs were calculated from the absorbance values of the organ extracts. Only liver, tumor, kidneys and spleen retained detectable cy-2-glu concentrations. Of note, the tumor was the second highest tissue for cy-2-glu accumulation. The absorbance values of cy-2-glu from all other organs were below the limit of detection.

Use of excess of D-glucose to reduce the uptake of cy-2-glu in liver

In order to reduce the uptake of cy-2-glu by the liver and improve tumor imaging, we performed a competitive inhibition experiment with 100 µL of 20 mM D-glucose in PBS via intravenous supplementation in nude mice. We anticipated that saturation of the liver with D-glucose, prior to administration of cy-2-glu could reduce the uptake of cy-2-glu by the liver and decrease fluorescence intensity from this organ. After D-glucose administration, the presence of cy-2-glu in the liver was visibly reduced at the 20 min and 4 hrs time points (Fig. 6a). However, the fluorescence intensity emanating from the liver was still too high and obscured the rest of the organs. Thus, the liver area was covered with a black strip and the exposure time was increased from 10 secs to 2 min to collect ample signal from the mammary tumor and other tissues. As seen from the images at 20 min and 4 hrs, fluorescence intensity was reduced when excess D-glucose was injected (Fig. 6b). At 24 hrs the effect of D-glucose pre-administration wore off and cy-2-glu accumulation in both mice was nearly equivalent. These results support our previous *in vitro* findings that cy-2-glu was capable of utilizing a glucose-based transport mechanism for entering the cells and suggest that this approach could be optimized in the future to improve cy-2-glu imaging.

Metabolic fate of the probes

To determine the retention time of cy-2-glu *in vivo* and discern the *in vivo* fate of the probe in mice, we analyzed urine extracts from mice treated with cy-2-glu. The absorbance data on the urine samples over a six day period indicated that the probe was continuously excreted from the body (Fig. 7a). Mass spectrometry data on specimens from mice after 24 hrs post-injection of cy-2-glu revealed a peak at 625 *m/z* (Fig. 7b), suggesting deamidation of cy-2-glu to cypate occurred during the excretion process. This supports our previous *in vitro* findings of cy-2-glu deamidation in liver cells (Fig. 4d).

Discussion:

Our study of the transport pathway and biodistribution of cy-2-glu and cypate demonstrates how imaging probes can be made to take advantage of cancer metabolism. Glucose is transported into cells through

glucose transport proteins (GLUTs). Malignancies promote blood vessel formation to increase oxygen and nutrient uptake. Consequently, malignant tissues may alter their metabolism and produce lactic acid through aerobic glycolysis. This lactic acid is responsible for the membrane translocation of GLUTs which in turn increases glucose uptake within the cells (Medina and Owen 2002). Thus, increased energy utilization promotes proliferation and leads to enhanced glucose uptake and overexpression of glucose transporters. Due to ligand promiscuity, mannose, galactose and glucosamine can also be transported via GLUTs (Calvo et al. 2010). In our study, we correlated cy-2-glu uptake in cancer cell lines with the GLUT overexpression on their surfaces. For example, A549 cells, which are reported to overexpress GLUT4 and GLUT1, have enhanced cy-2-glu uptake as compared to their normal counterpart, which does not express GLUT4 (O'Byrne et al. 2011; Ong et al. 2008). In prostate cells, GLUT1 expression increases with advanced malignancies (Effert et al. 2004). Based upon these previously published studies and the results obtained within this study, we can infer that the higher glucose requirement of cancer cells could increase cy-2-glu uptake in malignant cells as compared to normal, non-transformed counterparts.

Others reported that the addition of glucose can competitively inhibit glucosamine transport (Estensen and Plagemann 1972; Plagemann and Erbe 1973). We performed a similar competition experiment to demonstrate that cy-2-glu employs a glucose-utilizing transport pathway. Using D-glucose, the uptake of cy-2-glu was inhibited in cancer cells. In contrast, using a different cancer cell line, prostate cancer PC3-luc cells, Korotcov et al reported that cypate-glucosamine probe uptake was not affected by D-glucose (Korotcov et al. 2012). These different outcomes could result from cell-specific effects or the *in vitro* cell culture conditions used. Hence, cancer cells may possess distinct surface charges that affect macromolecule uptake. Another aspect that could impact the uptake of dyes like cypate was presented by Cheng et al., who suggested, using U87MG gliolblastoma cells, that a dye's molecular weight could affect its transport pathway (Cheng et al. 2006). Interestingly, in our cancer cells, we did not observe any change in glucosamine transport due to attachment of the large cypate molecule, while in non-cancer cell lines, the NIR signal was too low to detect any difference in cy-2-glu uptake in presence and absence of

D-glucose. The *in vivo* uptake of cy-2-glu in mice also displayed competitive inhibition by D-glucose during the first 4 hrs of the administration of cy-2-glu. Cy-2-glu accumulation showed a considerable reduction in the liver, and also in the tumor. Our intent in performing this experiment was to determine whether the liver would take up more pre-injected D-glucose from the blood than the tumor, competitively inhibiting cy-2-glu uptake and reducing the intensity of the very bright liver fluorescent signal. While this proved to be the case, fluorescent intensity of the cy-2glu signal in the tumor was also reduced. However, since Korotcov et al. performed similar *in vivo* studies and showed that no competitive inhibition of cypate-glucosamine occurred at 24 hrs post-injection with D-glucose, we also observed that at 24 hrs time point the inhibition effect of D-glucose wore off (Korotcov et al. 2012). It is possible that this approach to reduce liver fluorescence and improve detection of the tumor signal could work for other cancer cell lines with different metabolic profiles. While this can be evaluated in future studies, the presented *in vitro* and *in vivo* results confirm the use of GLUT-based pathway for cy-2-glu transport and uptake by cancer cells.

One reason for the difference in the *in vitro* uptake of cypate in cancer cells compared to normal cells could be the interaction of negatively charged cypate with the cell membrane. Cancer cells have less negatively charged surfaces than normal cells (Cook and Jacobson 1968; Zhang et al. 2008; Ambrose, James, and Lowick 1956; Purdom, Ambrose, and Klein 1958), which leads to reduced repulsion between cypate and the cancer cell surface, enhancing uptake. While in our *in vitro* studies, we observed that cypate and cy-2-glu were similarly taken up by the cancer cells, *in vivo* we found that the cypate accumulation in the tumor was less than the cy-2-glu accumulation. This was also reported by Korotcov et al. (Korotcov et al. 2012), who showed that amount of cypate taken up by cancer cells was less than the cypate-glucosamine conjugates. The reduced uptake of cypate in the tumor *in vivo*, compared to cy-2-glu, could be explained by the difference in the chemical structure of these two cypate forms. The protein makeup associated with cypate and cy-2-glu *in vivo* could influence their biodistribution pathways

differently and be dependent on chemical factors of hydrophobicity, charge, and available functional groups for interaction.

Understanding the transport pathway of cypate contributes new knowledge to help optimize the chemical structure of such dyes. To validate our assumption that cypate uses carboxylates for transport purposes *in vitro* and to be responsible for the differences in uptake between cancer and normal cell lines, we performed competitive uptake inhibition experiments using PA, the fatty acid known to use the fatty acid transport mechanism. Transport of fatty acids such as oleate, stearate, palmitate is facilitated by membrane transport proteins (Abumrad, Park, and Park 1984; Abumrad et al. 1981; Potter et al. 1987). Long chain fatty acids are mainly transported through CD36, plasma membrane-associated fatty acid-binding protein (FABPpm) and fatty acid transport proteins (FATPs) (Schwenk et al. 2008; Ehehalt et al. 2006; Su and Abumrad 2009). The decrease in the fluorescence intensity of cypate in the presence of excess PA suggested that the binding sites for fatty acid were blocked by PA and were unavailable for cypate, confirming the use of carboxylates by cypate. We synthesized a non-NIR fluorescent analog of cypate called sat-cy by adding four hydrogen atoms across the π-conjugated system in cypate interrupting the π-conjugation system responsible for NIR optical properties. The presence of an excess of sat-cy also led to a decrease in the fluorescence intensity of cypate. Both PA and sat-cy did not exhibit competitive inhibition for the uptake of cy-2-glu, in which the carboxylic acid is modified to an amide bond. Thus, cypate and sat-cy may use the membrane transport proteins employed by fatty acids for entering cells.

Guo et al. found that both cypate and the glucosamine conjugates were cleared from the body within 24 hrs (Jing et al. 2012), whereas Korotcov et al. showed that the retention time of the cypate-glucosamine conjugate was almost 96 hours (Korotcov et al. 2012). In our study we observed that cy-2-glu was retained in the animal for more than 6 days. This slow removal of cy-2-glu from the animal with increased tumor accumulation suggests that cy-2-glu could be a promising NIR probe for cancer detection and treatment monitoring. The biodistribution data revealed that, second to the liver, the tumor had considerable accumulation of cy-2-glu followed by the kidneys and spleen. Analysis of urine extracts by

absorption spectroscopy and mass spectrometry revealed that this probe was cleared from the body through renal excretion in the form of free cypate. It is possible that cy-2-glu undergoes hydrolysis in the liver, kidneys and spleen which produces glucosamine and the cypate that is subsequently excreted and detected in urine. This possible hydrolysis was examined by performing an *in vitro* experiment with THLE-2 liver cells incubated with cy-2-glu that showed the presence of free cypate as one of the excreted metabolites. The mass spectrometry data of the *in vitro* extracts of prostate cancer cells, as well as normal cells, revealed the presence of cypate, indicating deamidation of cy-2-glu. Fatty acid amide hydrolase (FAAH) and N-acylethanolamine acid amidase (NAAA) are the two main enzymes present in the animal tissue responsible for degradation of N-acylethanolamines into fatty acid and ethanolamine (Ueda et al. 1999; Cravatt et al. 1996; Sakura et al. 2016; Tsuboi et al. 2005; Tsuboi, Takezaki, and Ueda 2007; Ueda, Yamanaka, and Yamamoto 2001). Cy-2-glu likely undergoes deamidation by these enzymes and releases free glucosamine.

In summary, the presence of excess D-glucose was observed to competitively inhibit the amount of cy-2-glu taken up in cancer cells both *in vitro* and *in vivo*, indicating cy-2-glu transport likely occurs through a glucose-mediated pathway and that the attachment of a bulky molecule like cypate does not alter the transport pathway of glucosamine. The presence of excess sat-cy and PA competitively decreased the amount of cypate transported into the cells, indicating the probable use of carboxylate groups for transport via the fatty acid transport proteins. The long retention period and high accumulation of cy-2-glu in tumors along with the release of glucosamine through hydrolysis in the tissues, suggest that cy-2-glu has promising applications for preclinical animal imaging studies, especially with orthotopic and subcutaneous tumors, and with further optimization could have future translation use.

Disclosures None.

Acknowledgements

We would like to acknowledge Dr. Griffith Parks, The Interim Associate Dean for research, for providing us the frozen vials of A549, BPH, DU145 and MDA-MB-231 cell lines, Kunal Dhume, BSBS, UCF, for helping in statistical analysis, Alexander Bosak, BSBS, Internal Medicine, UCF, for helping in grammar editing, and Dr. Chandrakala Aluganti Narasimhulu, BSBS, College of Medicine, UCF.

Data availability

The raw/processed data required to reproduce these findings cannot be shared at this time as the data also forms part of an ongoing study.

Author contribution:

Participated in research design: M.Doshi, D. Nierenberg, O. Flores, A.R. Khaled, S. Parthasarathy

Conducted experiments: M.Doshi, D. Nierenberg, O. Flores, P. Deme,

Contributed new reagents or analytical tools:

Performed data analysis: M.Doshi, D. Nierenberg, P. Deme, E. Becerra

Wrote of contributed to the writing of the manuscript: M.Doshi, D. Nierenberg, P. Deme, A.R. Khaled, S. Parthasarathy

References:

Abumrad, N A, J H Park, and C R Park (1984) Permeation of long-chain fatty acid into adipocytes. Kinetics, specificity, and evidence for involvement of a membrane protein. Journal of Biological Chemistry, 259: 8945-53.

Abumrad, N A, R C Perkins, J H Park, and C R Park (1981) Mechanism of long chain fatty acid permeation in the isolated adipocyte. Journal of Biological Chemistry, 256: 9183-91.

Achilefu, S, S Bloch, M A Markiewicz, T Zhong, Y Ye, R B Dorshow, B Chance, and K Liang (2005) Synergistic effects of light-emitting probes and peptides for targeting and monitoring integrin expression. Proceedings of the National Academy of Sciences of the United States of America, 102: 7976-81.

Achilefu, S, R B Dorshow, J E Bugaj, and R Rajagopalan (2000) Novel receptor-targeted fluorescent contrast agents for in vivo tumor imaging. Investigative Radiology, 35: 479-85.

Ambrose, E J, A M James, and J H B Lowick (1956) Differences between the electrical charge carried by normal and homologous tumour cells. Nature, 177: 576.

Calvo, M B, A Figueroa, E G Pulido, R G Campelo, and L A Aparicio (2010) Potential role of sugar transporters in cancer and their relationship with anticancer therapy. International Journal of Endocrinology, 2010: 14.

Chan, K, M McMahon, G Liu, Y Kato, Z Bhujwalla, D Artemov, and P van Zijl. 2011. Imaging of glucose uptake in breast tumors using non-labeled d-glucose. Proceedings of the International Society of Magnetic Resonance in Medicine, 19th Meeting and Excibition, 551.

Cheng, Z, J Levi, Z Xiong, O Gheysens, S Keren, X Chen, and S S Gambhir (2006) Near-infrared fluorescent deoxyglucose analog for tumor optical imaging in cell culture and in living mice. Bioconjugate Chemistry, 17: 662-69.

Cook, G M W, and W Jacobson (1968) The electrophoretic mobility of normal and leukaemic cells of mice. Biochemical Journal, 107: 549-57.

660 Cravatt, B F, D K Giang, S P Mayfield, D L Boger, R A Lerner, and N B Gilula (1996) Molecular
661 characterization of an enzyme that degrades neuromodulatory fatty-acid amides. Nature, 384: 83-
662 87.
663 Donuru, V R, S Zhu, S Green, and H Liu (2010) Near-infrared emissive bodipy polymeric and
664 copolymeric dyes. Polymer, 51: 5359-68.
665 Effert, P, A J Beniers, Y Tamimi, S Handt, and G Jakse (2004) Expression of glucose transporter 1
666 (GLUT-1) in cell lines and clinical specimens from human prostate adenocarcinoma. Anticancer
667 Research, 24: 3057-64.
668 Ehehalt, R, J Füllekrug, J Pohl, A Ring, T Herrmann, and W Stremmel (2006) Translocation of long chain
669 fatty acids across the plasma membrane – lipid rafts and fatty acid transport proteins. Molecular
670 and Cellular Biochemistry, 284: 135-40.
671 Escobedo, J O, O Rusin, S Lim, and R M Strongin (2010) NIR dyes for bioimaging applications. Current
672 Opinion in Chemical Biology, 14: 64-70.
673 Estensen, R D, and P G W Plagemann (1972) Cytochalasin b: Inhibition of glucose and glucosamine
674 transport. Proceedings of the National Academy of Sciences of the United States of America, 69:
675 1430-34.
676 Flamen, P, A Lerut, E V Cutsem, W D Wever, M Peeters, S Stroobants, P Dupont, G Bormans, M Hiele,
677 P D Leyn, D V Raemdonck, W Coosemans, N Ectors, K Haustermans, and L Mortelmans (2000)
678 Utility of positron emission tomography for the staging of patients with potentially operable
679 esophageal carcinoma. Journal of Clinical Oncology, 18: 3202-10.
680 Hanahan, D, and Robert A Weinberg Hallmarks of cancer: The next generation. Cell, 144: 646-74.
681 Haque, A, M S H Faizi, J A Rather, and M S Khan (2017) Next generation NIR fluorophores for tumor
682 imaging and fluorescence-guided surgery: A review. Bioorganic & Medicinal Chemistry, 25:
683 2017-34.
684 Hilderbrand, S A, and R Weissleder (2010) Near-infrared fluorescence: Application to in vivo molecular
685 imaging. Current Opinion in Chemical Biology, 14: 71-79.

686 Hoh, C K, R A Hawkins, J A Glaspy, M Dahlbom, N Y Tse, E J Hoffman, C Schiepers, Y Choi, S Rege,
687 and E Nitzsche (1993) Cancer detection with whole-body pet using 2-[18F]fluoro-2-deoxy-d-
688 glucose. Journal of computer assisted tomography, 17: 582-89.
689 Jing, G, D Changli, S Lingling, Z Hongyan, X Bing, Q Zhiyu, A Samuel, and G Yueqing (2012)
690 Comparison of near-infrared fluorescent deoxyglucose probes with different dyes for tumor
691 diagnosis in vivo. Contrast Media & Molecular Imaging, 7: 289-301.
692 Kim, J S, R Kodagahally, L Strekowski, and G Patonay (2005) A study of intramolecular h-complexes of
693 novel bis(heptamethine cyanine) dyes. Talanta, 67: 947-54.
694 Korotcov, A V, Y Ye, Y Chen, F Zhang, S Huang, S Lin, R Sridhar, S Achilefu, and P C Wang (2012)
695 Glucosamine-linked near-infrared fluorescent probes for imaging of solid tumor xenografts.
696 Molecular Imaging and Biology, 14: 443-51.
697 Lapela, M, R Grénman, T Kurki, H Joensuu, S Leskinen, P Lindholm, M Haaparanta, U Ruotsalainen,
698 and H Minn (1995) Head and neck cancer: Detection of recurrence with PET and 2-[F-18]fluoro-
699 2-deoxy-d-glucose. Radiology, 197: 205-11.
700 Liberti, M V, and J W Locasale (2016) The Warburg effect: How does it benefit cancer cells?, Trends in
701 biochemical sciences, 41: 211-18.
702 Luo, S, E Zhang, Y Su, T Cheng, and C Shi (2011) A review of NIR dyes in cancer targeting and
703 imaging. Biomaterials, 32: 7127-38.
704 Medina, R A, and G I Owen (2002) Glucose transporters: Expression, regulation and cancer. Biological
705 Research, 35: 9-26.
706 Nakazumi, H, T Ohta, H Etoh, T Uno, C L Colyer, Y Hyodo, and S Yagi (2005) Near-infrared
707 luminescent bis-squaraine dyes linked by a thiophene or pyrene spacer for noncovalent protein
708 labeling. Synthetic Metals, 153: 33-36.
709 O'Byrne, K J, A-M Baird, L Kilmartin, J Leonard, C Sacevich, and S G Gray (2011) Epigenetic
710 regulation of glucose transporters in non-small cell lung cancer. Cancers, 3: 1550-65.

711 Ong, L C, Y Jin, I C Song, S Yu, K Zhang, L C Ong, Y Jin, I C Song, S Yu, K Zhang, and P K H Chow
712 (2008) 2-[18F]-2-deoxy-d-glucose (FDG) uptake in human tumor cells is related to the expression
713 of GLUT-1 and hexokinase II. Acta Radiologica, 49: 1145-53.
714 Owens, E A, M Henary, G El Fakhri, and H S Choi (2016) Tissue-specific near-infrared fluorescence
715 imaging. Accounts of Chemical Research, 49: 1731-40.
716 Peng, X, F Song, E Lu, Y Wang, W Zhou, J Fan, and Y Gao (2005) Heptamethine cyanine dyes with a
717 large stokes shift and strong fluorescence: A paradigm for excited-state intramolecular charge
718 transfer. Journal of the American Chemical Society, 127: 4170-71.
719 Phelps, M E (2000) Positron emission tomography provides molecular imaging of biological processes.
720 Proceedings of the National Academy of Sciences, 97: 9226-33.
721 Plagemann, P G, and J Erbe (1973) Transport and metabolism of glucosamine by cultured novikoff rat
722 hepatoma cells and effects on nucleotide pools. Cancer research, 33: 482-92.
723 Potter, B J, D Stump, W Schwieterman, D Sorrentino, L N Jacobs, C L Kiang, J H Rand, and P D Berk
724 (1987) Isolation and partial characterization of plasma membrane fatty acid binding proteins from
725 myocardium and adipose tissue and their relationship to analogous proteins in liver and gut.
726 Biochemical and Biophysical Research Communications, 148: 1370-76.
727 Purdom, L, E J Ambrose, and G Klein (1958) A correlation between electrical surface charge and some
728 biological characteristics during the stepwise progression of a mouse sarcoma. Nature, 181: 1586.
729 Rivlin, M, and G Navon (2018) CEST MRI of 3-O-methyl-D-glucose on different breast cancer models.
730 Magnetic Resonance in Medicine, 79: 1061-69.
731 Sakura, Y, K Tsuboi, T Uyama, X Zhang, R Taoka, M Sugimoto, Y Kakehi, and N Ueda (2016) A
732 quantitative study on splice variants of N-acylethanolamine acid amidase in human prostate
733 cancer cells and other cells. Biochimica et Biophysica Acta (BBA) - Molecular and Cell Biology
734 of Lipids, 1861: 1951-58.
735 Schwenk, R W, J J F P Luiken, A Bonen, and J F C Glatz (2008) Regulation of sarcolemmal glucose and
736 fatty acid transporters in cardiac disease. Cardiovascular Research, 79: 249-58.

737 Som, P, H L Atkins, D Bandoypadhyay, J S Fowler, R R MacGregor, K Matsui, Z H Oster, D F Sacker, C
738 Y Shiue, H Turner, C-N Wan, A P Wolf, and S V Zabinski (1980) A fluorinated glucose analog,
739 2-fluoro-2-deoxy-d-glucose (F-18): Nontoxic tracer for rapid tumor detection. Journal of
740 computer assisted tomography, 4: 878.
741 Srinivasan, A, T Ishizuka, A Osuka, and H Furuta (2003) Doubly n-confused hexaphyrin: A novel
742 aromatic expanded porphyrin that complexes bis-metals in the core. Journal of the American
743 Chemical Society, 125: 878-79.
744 Su, X, and N A Abumrad (2009) Cellular fatty acid uptake: A pathway under construction. Trends in
745 endocrinology and metabolism: TEM, 20: 72-77.
746 Tanaka, Y, J-Y Shin, and A Osuka (2008) Facile synthesis of large meso-pentafluorophenyl-substituted
747 expanded porphyrins. European Journal of Organic Chemistry, 2008: 1341-49.
748 Tsuboi, K, Y-X Sun, Y Okamoto, N Araki, T Tonai, and N Ueda (2005) Molecular characterization of N-
749 acylethanolamine-hydrolyzing acid amidase, a novel member of the choloylglycine hydrolase
750 family with structural and functional similarity to acid ceramidase. Journal of Biological
751 Chemistry, 280: 11082-92.
752 Tsuboi, K, N Takezaki, and N Ueda (2007) The N-acylethanolamine-hydrolyzing acid amidase (NAAA).
753 Chemistry & Biodiversity, 4: 1914-25.
754 Ueda, N, K Yamanaka, Y Terasawa, and S Yamamoto (1999) An acid amidase hydrolyzing anandamide
755 as an endogenous ligand for cannabinoid receptors. FEBS Letters, 454: 267-70.
756 Ueda, N, K Yamanaka, and S Yamamoto (2001) Purification and characterization of an acid amidase
757 selective for N-palmitoylethanolamine, a putative endogenous anti-inflammatory substance.
758 Journal of Biological Chemistry, 276: 35552-57.
759 Umezawa, K, D Citterio, and K Suzuki (2008) Water-soluble nir fluorescent probes based on squaraine
760 and their application for protein labeling. Analytical Sciences, 24: 213-17.

761 Umezawa, K, A Matsui, Y Nakamura, D Citterio, and K Suzuki (2009) Bright, color-tunable fluorescent
762 dyes in the VIS/NIR region: Establishment of new “tailor-made” multicolor fluorophores based
763 on borondipyrromethene. Chemistry – A European Journal, 15: 1096-106.
764 Umezawa, K, Y Nakamura, H Makino, D Citterio, and K Suzuki (2008) Bright, color-tunable fluorescent
765 dyes in the visible−near-infrared region. Journal of the American Chemical Society, 130: 1550-
766 51.
767 Vinogradov, E, A D Sherry, and R E Lenkinski (2013) CEST: From basic principles to applications,
768 challenges and opportunities. Journal of Magnetic Resonance, 229: 155-72.
769 Volkova, K D, V B Kovalska, A L Tatarets, L D Patsenker, D V Kryvorotenko, and S M Yarmoluk
770 (2007) Spectroscopic study of squaraines as protein-sensitive fluorescent dyes. Dyes and
771 Pigments, 72: 285-92.
772 Walker-Samuel, S, R Ramasawmy, F Torrealdea, M Rega, V Rajkumar, S P Johnson, S Richardson, M
773 Gonçalves, H G Parkes, E Årstad, D L Thomas, R B Pedley, M F Lythgoe, and X Golay (2013)
774 In vivo imaging of glucose uptake and metabolism in tumors. Nature medicine, 19: 1067-72.
775 Warburg, O (1925) The metabolism of carcinoma cells. The Journal of Cancer Research, 9: 148.
776 Warburg, O (1956) On the origin of cancer cells. Science, 123: 309-14.
777 Wu, B, G Warnock, M Zaiss, C Lin, M Chen, Z Zhou, L Mu, D Nanz, R Tuura, and G Delso (2016) An
778 overview of CEST MRI for non-mr physicists. EJNMMI Physics, 3: 19.
779 Xie, Y-S, K Yamaguchi, M Toganoh, H Uno, M Suzuki, S Mori, S Saito, A Osuka, and H Furuta (2009)
780 Triply n-confused hexaphyrins: Near-infrared luminescent dyes with a triangular shape.
781 Angewandte Chemie International Edition, 48: 5496-99.
782 Ye, Y, S Bloch, J Kao, and S Achilefu (2005) Multivalent carbocyanine molecular probes: Synthesis and
783 applications. Bioconjugate Chemistry, 16: 51-61.
784 Zhang, S, R Trokowski, and A D Sherry (2003) A paramagnetic CEST agent for imaging glucose by
785 MRI. Journal of the American Chemical Society, 125: 15288-89.

Zhang, Y, M Yang, N G Portney, D Cui, G Budak, E Ozbay, M Ozkan, and C S Ozkan (2008) Zeta potential: A surface electrical characteristic to probe the interaction of nanoparticles with normal and cancer human breast epithelial cells. Biomedical Microdevices, 10: 321-28.

Scheme 1: Chemical **s**tructures of cypate, glucosamine, cy-1-glu and cy-2-glu

Figure legends:

Fig. 1: Presence of excess D-glucose competes with cy-2-glu for uptake in cells lines. Confocal fluorescence and corresponding DIC (diffraction interference contrast) images of the cell lines incubated with cy-2-glu (**a**) or cypate (**b**) in presence or absence of excess D-glucose. Green color represents the fluorescence from cy-2-glu or cypate. Solution spectroscopy data on cell extracts for cy-2-glu (**c,d**) or cypate (**e,f**). (**c**) represents cy-2-glu absorbance values in absence (red) or presence (grey) of D-glucose, while (**d**) represents cy-2-glu fluorescence values in absence (green) or presence of D-glucose (grey). (**e**) and (**f**) represents cypate absorbance or fluorescence, respectively, in the same manner as graphs (**c**) and (**d**). ** P<0.01, *** P<0.001, **** P<0.0001. Error bars represent standard deviation (n=3).

Fig. 2: Sat-cy and PA compete for internalization with cypate. Confocal fluorescence and corresponding DIC images of A549 cell line with cy-2-glu (**a**) and cypate (**b)**, in the presence or absence of excess D-glucose (glu), sat-cy and PA. (**c**) represents cy-2-glu absorbance spectra, while (**d**) represents cy-2-glu fluorescence spectra. Cypate absorbance and fluorescence spectra in (**e**) and (**f**) are represented in the same manner as (**c**) and (**d**), respectively. Cy-2-glu and cypate were extracted from the A549 cell lines (n=3).

Fig. 3: Synthesis and characterization of sat-cy. Reduction of cypate with Pd/C (10% Pd) in ethanol and passing hydrogen gas through the solution, to form sat-cy (**a**). Mass spectra of cypate at *m/z* 625 (**b**) and at *m/z* 629 for sat-cy (**c**). Absorbance spectra (**d**) and fluorescence spectra (**e**) of cypate (red line) and sat-cy (black line).

Fig. 4: Hydrolysis of cy-2-glu observed in prostate and liver cell lines. Mass spectra of dyes extracted from cancer and normal cell lines. Extractions from cell lines incubated with cy-2-glu (**a).** A549 and MRC9 show the ion at *m/z* 947 corresponding to cy-2-glu, while DU145 and BPH show the ions at *m/z* 947 and 625, corresponding to cy-2-glu and cypate, respectively. Extractions from cell lines incubated

with cypate (**b**). The ion at *m/z* 625 corresponding to cypate is observed in all the cell lines. The representative LC-HRMS extracted ion chromatograms of cypate at *m/z* 625.3629 ([M-H] ion) (**c,d,e**). Liver cell line THLE-2 incubated with (**c**) cypate, (**d**) cy-2-glu, (**c**) control and media evaluated for presence of cypate. Corresponding mass spectra of extracted ion chromatograms (**f**).

Fig 5: Retention and biodistribution of cy-2-glu and cypate over 6-days duration. *In vivo* images of nude mice bearing MDA-MB-231-luc2 tumors administered with cy-2-glu (**a**) and cypate (**b**). The liver area is covered with a black strip to block the strong fluorescence signal. Imaging for cy-2-glu injection was performed at 1 hr post-injection, followed by 24 hr periods for 6 days, while for cypate at 24 hr post-injection. Green color indicates cy-2-glu/cypate fluorescence, red color indicates bioluminescence from tumor due to luciferase expression, and grey color represents the reflectance image. An overlay of these images yields colocalization of cy-2-glu/cypate in tumors (yellow color). ***Ex vivo* imaging.** Fluorescence (**c**) and corresponding reflectance (**d**) images of organs isolated from mice at each time point (excitation wavelength – 760 nm, emission – 830 nm LP). Red indicates the highest, while blue indicates the lowest fluorescence intensity. The organs are placed in the order shown in **g**. **Biodistribution in organs**. Absorbance values of extracted probes plotted in bar graphs for each time point (**e**). Concentrations of cy-2-glu in liver, spleen, tumor and kidney (**f**), as calculated from the absorbance values obtained from **e** and from the calibration curve of cy-2-glu concentrations (Supplementary Fig 6). Error bars represent standard deviation (n=3 mice per group).

Fig. 6: *In vivo* competitive effect of glucose on cy-2-glu uptake. Images of mice at 20 min, 4 hrs and 24 hrs post-injection of cy-2-glu. Green color represents fluorescence of cy-2-glu, red color represents bioluminescence from the tumor and grey is the reflectance image. (Cy-2-glu + glucose) indicates injection of excess D-glucose 15 min prior to administration of cy-2-glu. Overlay of fluorescence and reflectance images showing cy-2-glu in the liver (exposure time: 10 sec) (**a**). Overlay of fluorescence, bioluminescence and reflectance images showing co-localization of cy-2-glu and the tumor in yellow color (**b**). In **b** liver is covered with a black strip (exposure time: 2 min). (n=2 mice/group)

Fig. 7: Characterization of the urine extracts. Absorbance values at 784 nm for cy-2-glu/cypate extracted from urine at increasing time points (**a**). Mass spectrometry data on urine extracts of mice injected with cy-2-glu at 24 hr time point showing molecular ion peak at 625 m/z for cypate. Error bars represent standard deviation (n=3 mice per group).

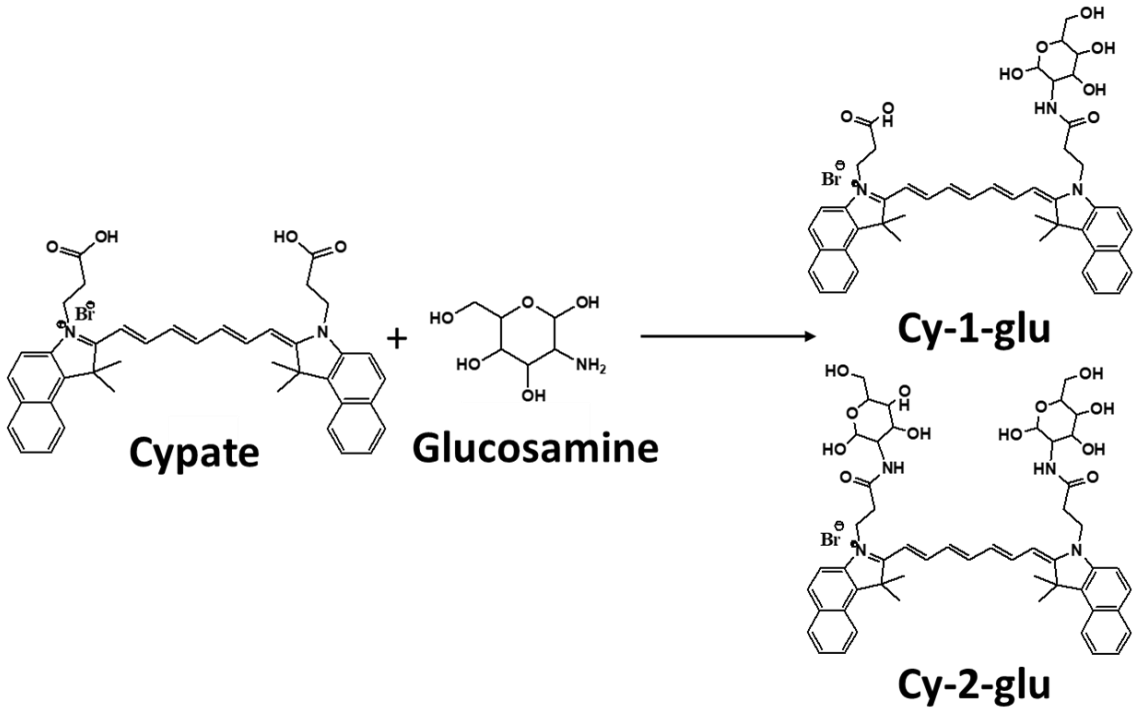

Scheme 1

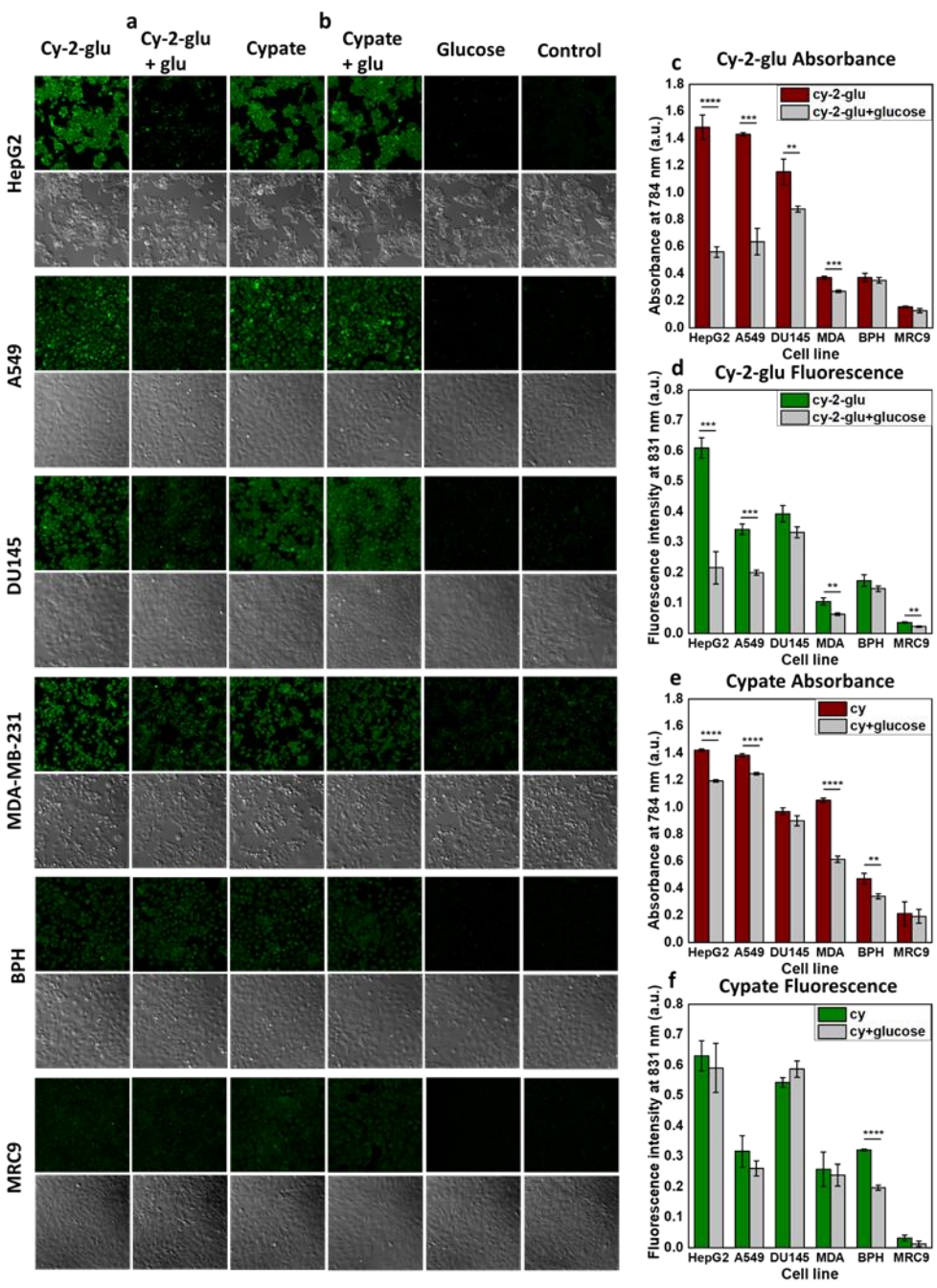
a
b
Cy-2-glu
Cy-2-glu + glu
Cypate
Cypate + glu
Glucose
Control
HepG2
A549
DU145
MDA-MB-231
BPH
MRC9
c
Cy-2-glu Absorbance
cy-2-glu
cy-2-glu+glucose
Absorbance at 784 nm (a.u.)
HepG2 A549 DU145 MDA BPH MRC9
Cell line
d
Cy-2-glu Fluorescence
Fluorescence intensity at 831 nm (a.u.)
e
Cypate Absorbance
cy
cy+glucose
f
Cypate Fluorescence

Fig 1

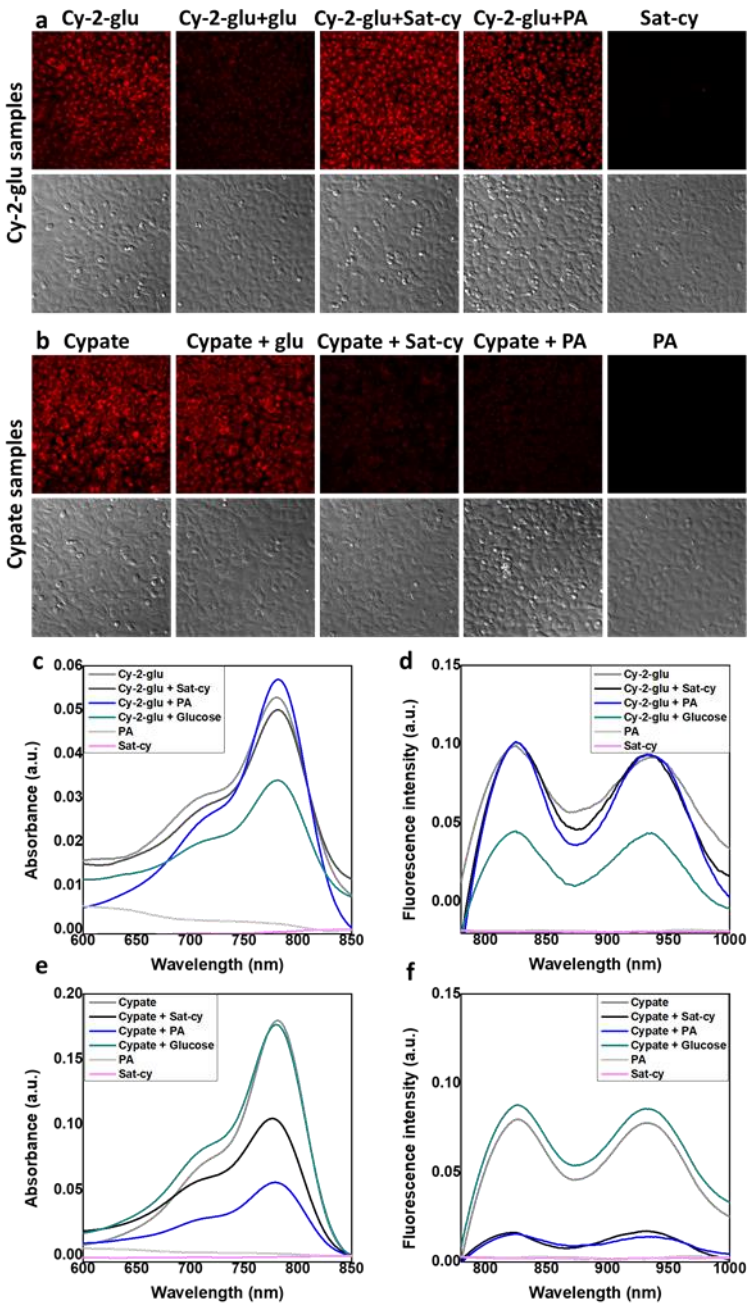
a
Cy-2-glu
Cy-2-glu+glu
Cy-2-glu+Sat-cy
Cy-2-glu+PA
Sat-cy
Cy-2-glu samples
b
Cypate
Cypate + glu
Cypate + Sat-cy
Cypate + PA
PA
Cypate samples
c
Absorbance (a.u.)
Wavelength (nm)
Cy-2-glu
Cy-2-glu + Sat-cy
Cy-2-glu + PA
Cy-2-glu + Glucose
PA
Sat-cy
d
Fluorescence intensity (a.u.)
Wavelength (nm)
e
Absorbance (a.u.)
Wavelength (nm)
Cypate
Cypate + Sat-cy
Cypate + PA
Cypate + Glucose
PA
Sat-cy
f
Fluorescence intensity (a.u.)
Wavelength (nm)

Fig 2

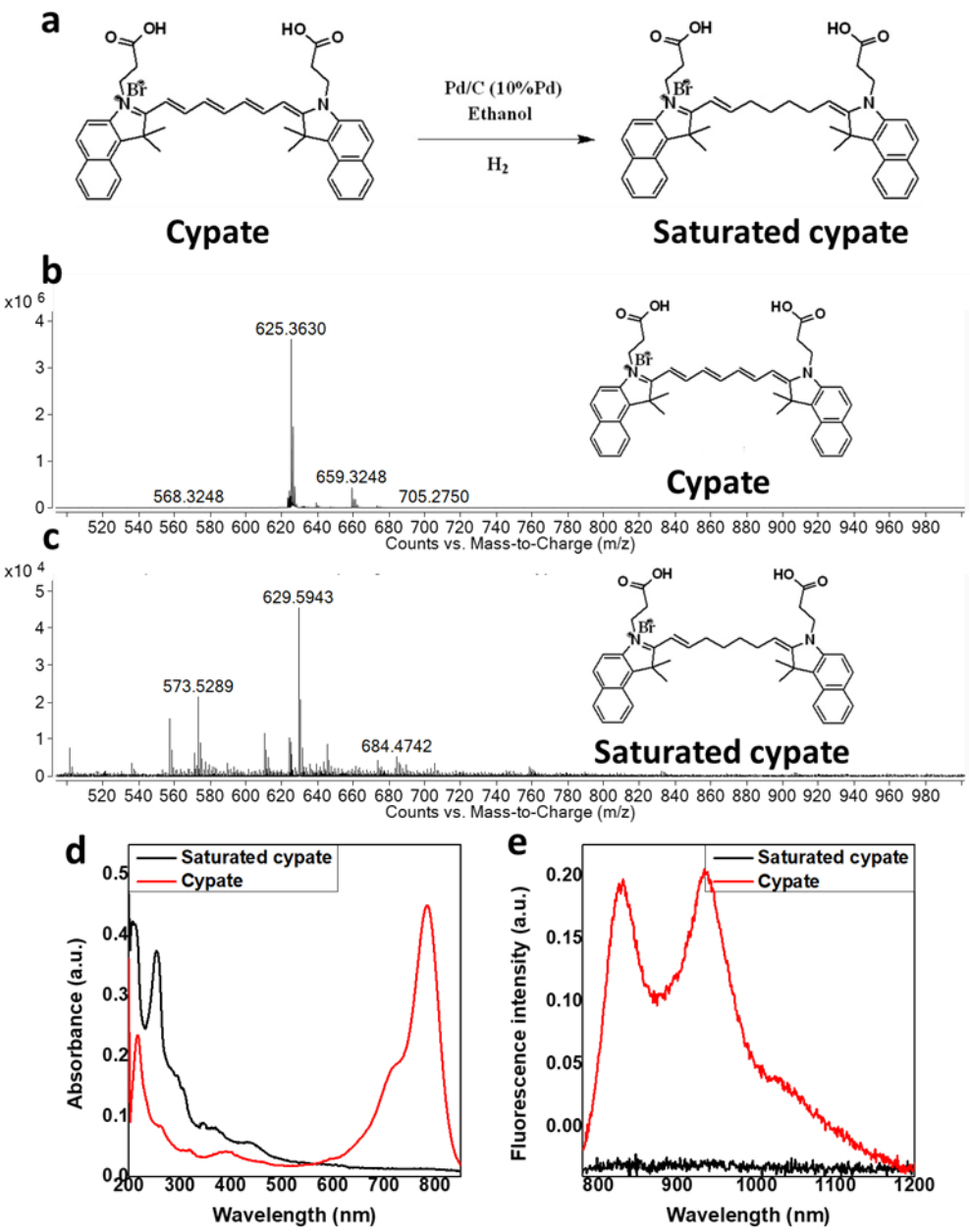
a
Pd/C (10%Pd)
Ethanol
H2
Cypate
Saturated cypate
b
625.3630
659.3248
568.3248
705.2750
Cypate
Counts vs. Mass-to-Charge (m/z)
c
629.5943
573.5289
684.4742
Saturated cypate
Counts vs. Mass-to-Charge (m/z)
d
Saturated cypate
Cypate
Absorbance (a.u.)
Wavelength (nm)
e
Saturated cypate
Cypate
Fluorescence intensity (a.u.)
Wavelength (nm)

Fig 3

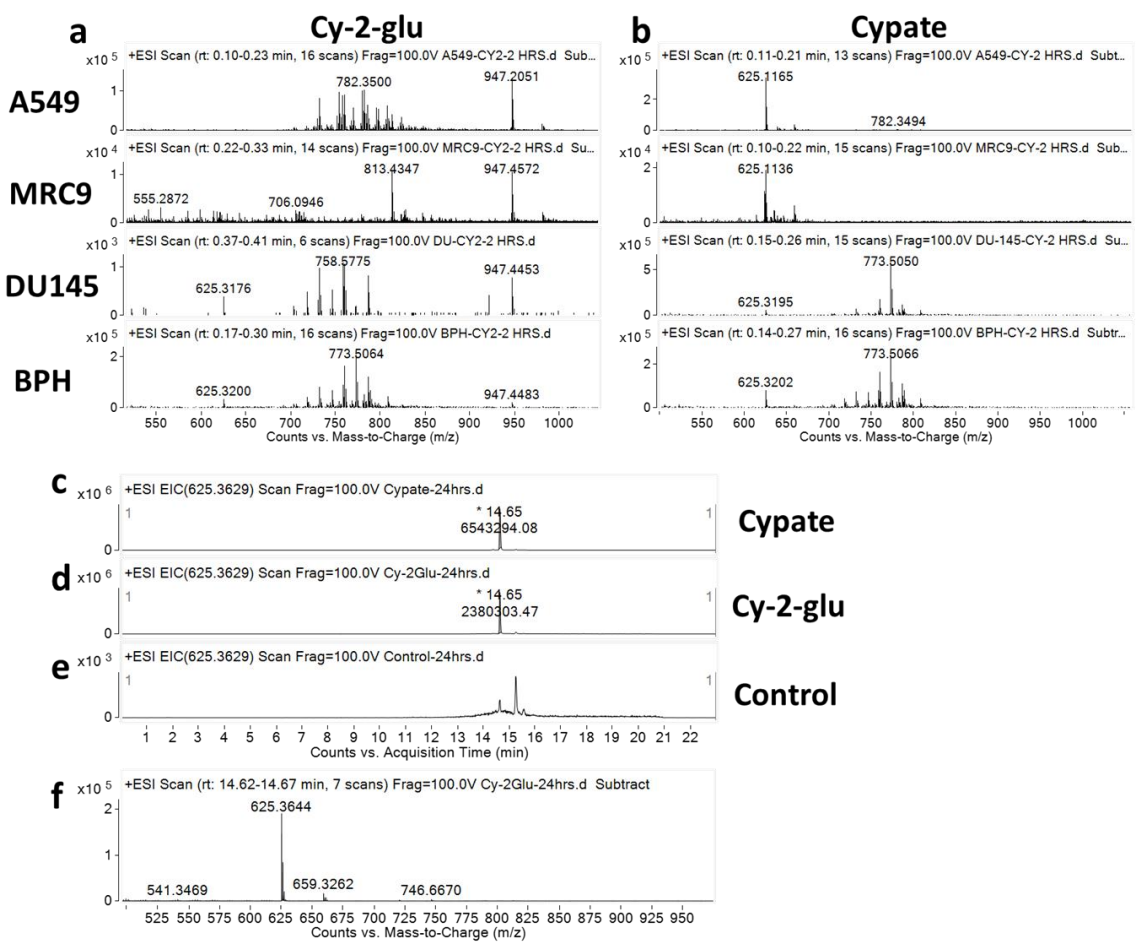
a
Cy-2-glu
b
Cypate
A549
MRC9
DU145
BPH
+ESI Scan (rt: 0.10-0.23 min, 16 scans) Frag=100.0V A549-CY2-2 HRS.d Sub...
782.3500
947.2051
+ESI Scan (rt: 0.22-0.33 min, 14 scans) Frag=100.0V MRC9-CY2-2 HRS.d Su...
813.4347
947.4572
555.2872
706.0946
+ESI Scan (rt: 0.37-0.41 min, 6 scans) Frag=100.0V DU-CY2-2 HRS.d
758.5775
947.4453
625.3176
+ESI Scan (rt: 0.17-0.30 min, 16 scans) Frag=100.0V BPH-CY2-2 HRS.d
773.5064
625.3200
947.4483
Counts vs. Mass-to-Charge (m/z)
+ESI Scan (rt: 0.11-0.21 min, 13 scans) Frag=100.0V A549-CY-2 HRS.d Subt...
625.1165
782.3494
+ESI Scan (rt: 0.10-0.22 min, 15 scans) Frag=100.0V MRC9-CY-2 HRS.d Sub...
625.1136
+ESI Scan (rt: 0.15-0.26 min, 15 scans) Frag=100.0V DU-145-CY-2 HRS.d Su...
773.5050
625.3195
+ESI Scan (rt: 0.14-0.27 min, 16 scans) Frag=100.0V BPH-CY-2 HRS.d Subtr...
773.5066
625.3202
Counts vs. Mass-to-Charge (m/z)
c
+ESI EIC(625.3629) Scan Frag=100.0V Cypate-24hrs.d
* 14.65
6543294.08
Cypate
d
+ESI EIC(625.3629) Scan Frag=100.0V Cy-2Glu-24hrs.d
* 14.65
2380303.47
Cy-2-glu
e
+ESI EIC(625.3629) Scan Frag=100.0V Control-24hrs.d
Control
Counts vs. Acquisition Time (min)
f
+ESI Scan (rt: 14.62-14.67 min, 7 scans) Frag=100.0V Cy-2Glu-24hrs.d Subtract
625.3644
541.3469
659.3262
746.6670
Counts vs. Mass-to-Charge (m/z)

Fig 4

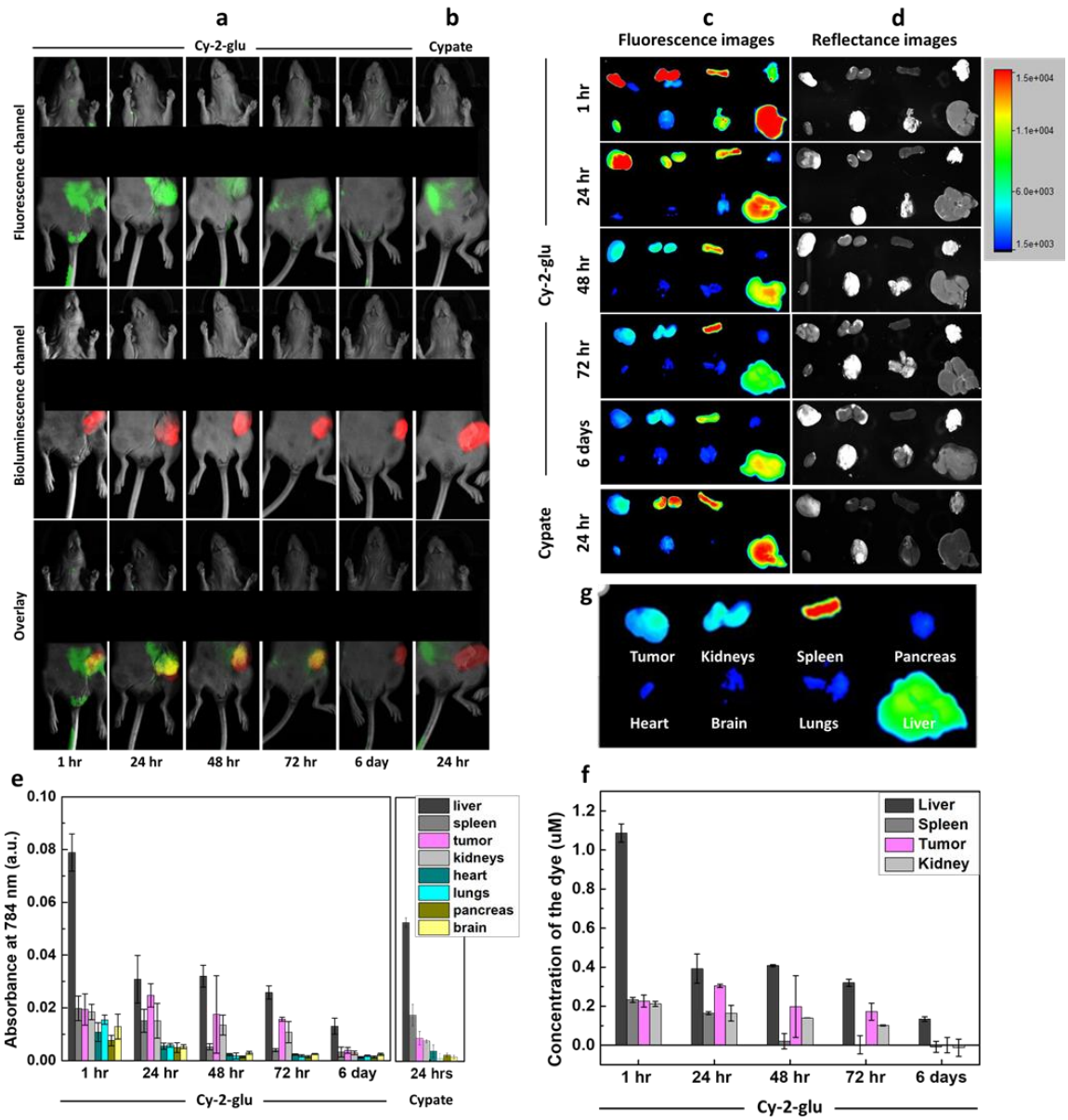
a
b
Cy-2-glu
Cypate
Fluorescence channel
Bioluminescence channel
Overlay
1 hr
24 hr
48 hr
72 hr
6 day
24 hr
c
Fluorescence images
d
Reflectance images
1 hr
24 hr
48 hr
72 hr
6 days
24 hr
Cy-2-glu
Cypate
1.5e+004
1.1e+004
6.0e+003
1.5e+003
g
Tumor
Kidneys
Spleen
Pancreas
Heart
Brain
Lungs
Liver
e
Absorbance at 784 nm (a.u.)
0.10
0.08
0.06
0.04
0.02
0.00
liver
spleen
tumor
kidneys
heart
lungs
pancreas
brain
1 hr
24 hr
48 hr
72 hr
6 day
24 hrs
Cy-2-glu
Cypate
f
Concentration of the dye (uM)
1.2
1.0
0.8
0.6
0.4
0.2
0.0
Liver
Spleen
Tumor
Kidney
1 hr
24 hr
48 hr
72 hr
6 days
Cy-2-glu

Fig 5

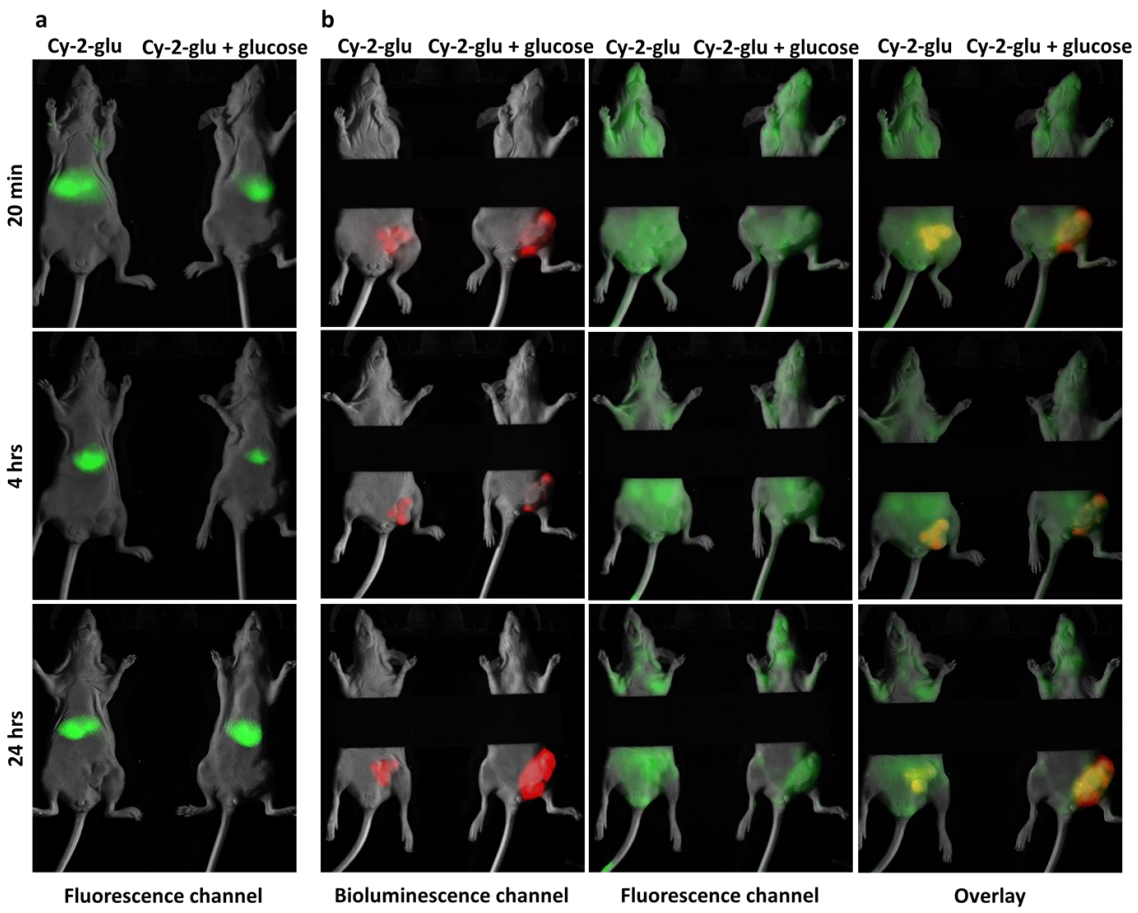
a
b
Cy-2-glu
Cy-2-glu + glucose
Cy-2-glu
Cy-2-glu + glucose
Cy-2-glu
Cy-2-glu + glucose
20 min
4 hrs
24 hrs
Fluorescence channel
Bioluminescence channel
Fluorescence channel
Overlay

Fig 6

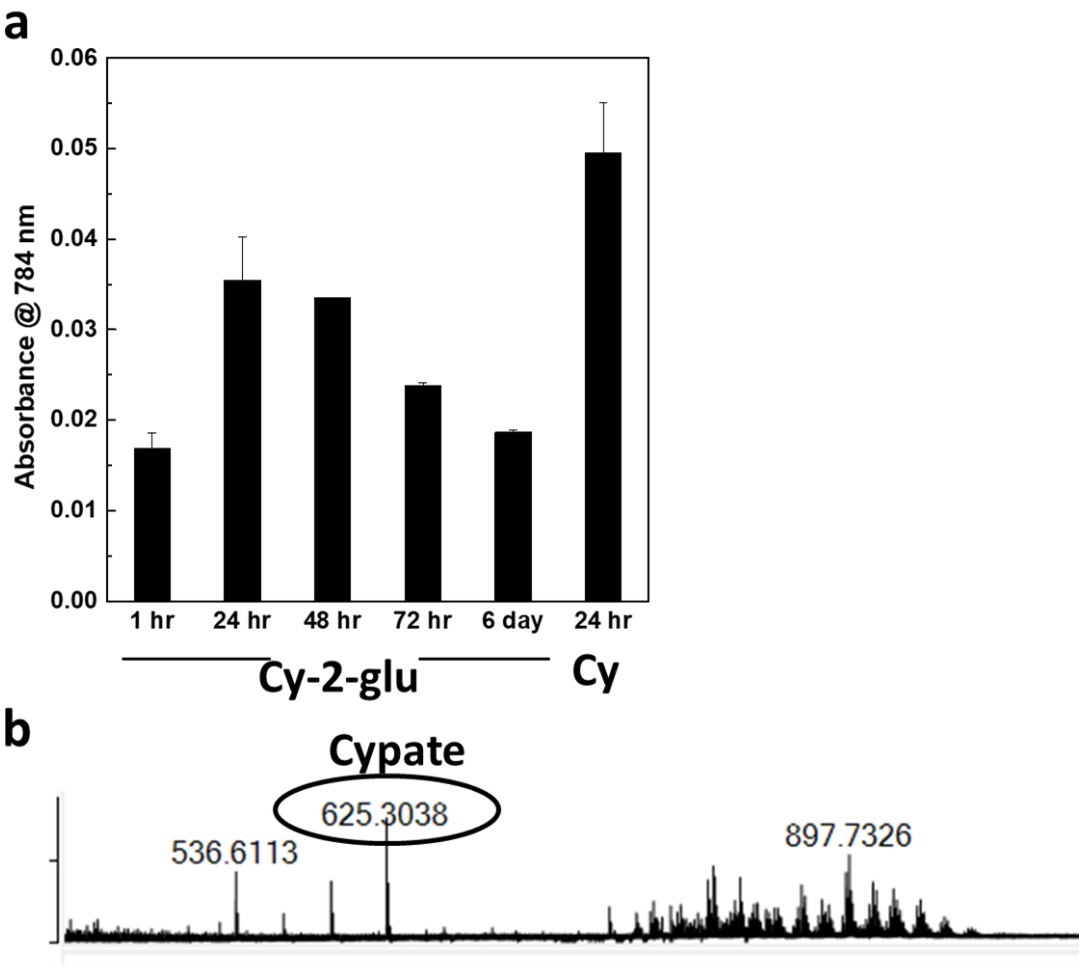
a
0.06
0.05
0.04
0.03
0.02
0.01
0.00
Absorbance @ 784 nm
1 hr
24 hr
48 hr
72 hr
6 day
24 hr
Cy-2-glu
Cy
b
Cypate
625.3038
536.6113
897.7326

Fig 7